ROYAL SOCIETY
OF CHEMISTRY

COMMUNICATION

Check for updates

Sucrose-derived carbon-coated nickel oxide (SDCC-NiO) as an electrode material for supercapacitor applications

Rahul Kumar, [iD] *[a] Ankur Soam[b] and Veena Sahajwalla[a]

Sucrose-derived carbon-coated nickel oxide (SDCC-NiO) was successfully synthesized *via* a colloidal method. Nickel oxide and sucrose were used to synthesize SDCC-NiO, where sucrose worked as a soluble source of carbon in the process. Sucrose was converted into carbon during annealing in an inert atmosphere and coated on the surface of nickel particles. SDCC-NiO was characterized *via* Brunauer–Emmett–Teller (BET) method, X-ray diffraction (XRD), Raman spectroscopy, scanning electron microscopy (SEM), transmission electron microscopy (TEM), and X-ray photoelectron spectroscopy (XPS). The as-prepared SDCC-NiO was used as an electrode material. SDCC-NiO exhibited the maximum specific capacitance of 473 F g^{-1} at a scan rate of 5 mV s^{-1} in a 1 M KOH electrolyte with an energy density of 4.5 kW kg^{-1} at a current density of 15 A g^{-1}.

1. Introduction

The industry of hybrid electric vehicles and portable electronic devices is growing rapidly and there is a need for high-power energy storage devices to fulfill the urgent demand for a sustainable energy system.[1] Supercapacitors have excited a great scientific interest due to their applications in energy storage. The merits of supercapacitors comprise high power density and a long lifespan. Moreover, supercapacitors are safe, cheap, and maintenance-free.[2] Electrode materials play an important role in the performance of supercapacitors. Carbon-based materials such as activated carbon, carbon fibers, carbon nanotubes, and graphene have been used as electrode materials for electric double-layer capacitors (EDLCs) due to high surface area and long cycling life stability.[3–5] However, transition-metal oxides such as RuO$_2$, MnO$_2$, NiO,

Co$_3$O$_4$, ZnO, SnO$_2$, and TiO$_2$ and conducting polymeric materials such as (polyaniline (PANI), polythiophene, and polypyrrole (PPy)) have been used as electrode materials for pseudocapacitors due to their much higher energy storage capacity than carbon-based materials.[6–23] Among transition-metal oxides, nickel oxide/hydroxide with its high theoretical capacitance, environment-friendly nature, high thermal stability, and abundance has been considered as one of the most promising candidates. However, the high resistivity of pure nickel oxide leads to poor rate capability and cycle stability, which has extremely limited its practical applications.[24–27] The capacitance of carbon-based supercapacitors can be improved by metal oxides, which can also contribute pseudo-capacitance apart from the double-layer capacitance of carbon materials.[28] Therefore, it is beneficial to combine metal oxides with carbon materials to develop hybrid materials that could incorporate the merits of both components and reduce the shortcomings of each component. This combination could improve the performance of SCs to meet energy storage demands in a sustainable way.[28–30]

Zhang *et al.* prepared monolithic NiO aerogels *via* a facile citric acid-assisted sol–gel method and this material exhibited the maximum specific capacitance of 797 F g^{-1} at a scan rate of 10 mV s^{-1}.[31] Yuan *et al.* fabricated the graphene oxide/nickel oxide glassy electrode *via* electrodeposition, and this material showed the maximum specific capacitance of 890 F g^{-1} at a scan rate of 5 mV s^{-1}.[32] Liu *et al.* prepared a nanocomposite based on NiO nanosheets with controllable size and thickness on carbon cloth *via* a cost-effective and scalable chemical precipitation method. This material exhibited the maximum specific capacitance of 600.3 F g^{-1} at a scan rate of 1 A g^{-1}.[33]

Zhu *et al.* synthesized a reduced graphene oxide/Ni oxide composite *via* homogeneous co-precipitation and this composite exhibited the maximum specific capacitance of 770 F g^{-1} at a scan rate of 2 mV s^{-1}.[34] Dar *et al.* studied the morphology and property control of NiO nanostructures prepared *via* electrodeposition (nanorods, nanotubes, and nanoporous films). These nanostructures exhibited the maximum specific capacitance

[a] Centre for Sustainable Materials Research and Technology, School of Materials Science and Engineering, SMaRT, University of New South Wales, NSW 2052, Australia. E-mail: kumarrahul003@gmail.com

[b] Department of Mechanical Engineering, Siksha 'O' Anusandhan University, Khandagiri Square, Bhubaneswar-751030, Odisha, India

of 797, 2093, and 1208 F g^{-1} at a scan rate of 5 mV s^{-1}.[35] Wang *et al.* fabricated NiO nanoflakes *via* a simple hydrothermal method on 3D (three-dimensional) graphene scaffolds grown on Ni foams by microwave plasma-enhanced chemical vapor deposition (MPCVD). The NiO 3D graphene hierarchical composite exhibited the maximum specific capacitance of 1681 F g^{-1} at a scan rate of 10 mV s^{-1}.[36]

Sun *et al.* fabricated porous nickel oxide nanosheets by synthesizing porous Ni(OH)$_2$ sheets using surfactant-templated wet chemistry, followed by the decomposition of hydroxides to oxides upon heat treatment. Nickel oxide nanosheets showed the maximum specific capacitance of 866.7 F g^{-1} at a scan rate of 5 mV s^{-1}.[37]

Iwueke *et al.* fabricated Ni(OH)$_2$/CuO nanocomposite thin films by successive ionic layer adsorption and reaction-deposited cupric oxide for supercapacitive applications. This nanocomposite thin film exhibited the maximum specific capacitance of 27 F g^{-1} at a scan rate of 10 mV s^{-1}.[38]

In this study, sucrose-derived carbon-coated nickel oxide (SDCC-NiO) has been investigated as an electrode material for supercapacitor applications. SDCC-NiO was fabricated using nickel oxide with the addition of sucrose. Sucrose was converted into carbon and coated on nickel oxide particles with heat treatment at a moderate temperature. The electrochemical performance of SDCC-NiO was evaluated *via* cyclic voltammetry and charging/discharging processes at a constant current.

2. Experimental

2.1. Fabrication of SDCC-NiO

Sucrose (Merck-Germany) and nickel oxide (Sigma Aldrich) were used to fabricate SDCC-NiO. First, PVA (1 wt%) (Sigma Aldrich, Mol. Weight = 100 000) solution was prepared in water and then sucrose was added into the solution. PVA was used as a binder for the fabrication of SDCC-NiO.[39–41] Nickel oxide was added to the sucrose-containing solution separately. This mixture was put on the magnetic stirrer for 24 h for stirring. The homogeneous suspension of nickel oxide was obtained, and the suspension was dried at 150 °C in an oven for 24 h to remove the water. After drying and crushing the mixture, sucrose-coated powder of nickel oxide was obtained. The annealing of sucrose-coated nickel oxide powder was done in flowing argon at 600 °C and dwell for 2 h to pyrolyze sucrose.[42] Thereafter, sucrose yielded 8 wt% of carbon in SDCC-NiO after annealing. The electrochemical properties of the annealed powder (SDCC-NiO) were investigated *via* cyclic voltammetry and charging/discharging processes at a constant current.

2.2. Characterization

The properties of SDCC-NiO were investigated using various equipment such as multi-point Brunauer–Emmett–Teller (BET), X-ray diffractometer (XRD, Model-PANalytical X'Pert Pro multipurpose XRD), Raman spectroscope (HORIBA Jobin Yvon LabRAM HR spectroscope), scanning electron microscope (SEM, Model-TM 3000 Hitachi), transmission electron microscope

(TEM, Model-JEOL JEM-2100 F), and X-ray photoelectron spectroscope (XPS, Model-Thermo ESCALAB250i).

The electrochemical properties of the SDCC-NiO electrode were measured *via* cyclic voltammetry (CV), galvanostatic charge–discharge (GC–D) measurements and electrochemical impedance spectroscopy (EIS) on Autolab potentiostat/galvanostatic (Biologic VSP-300) electrochemical workstation with a three-electrode cell. All the CV tests were performed between 0.0 to +0.6 V at different scan rates of 5–50 mV s^{-1}. The galvanostatic charge/discharge curves were investigated in the potential range of 0.0 to +0.6 V at current densities of 5–15 A g^{-1}.

3. Results and discussion

3.1. Surface, XRD, Raman, morphology and chemical compositional analysis of SDCC-NiO

The nitrogen adsorption/desorption experiment was done for SDCC-NiO, and the corresponding isotherm and pore size distribution is shown in Fig. 1(a and b). Micropore surface area and pore volume were determined using the *t*-plot method, and the micropore diameter was determined using the Dubinine-Astakhov (DA) method. The nitrogen adsorption/desorption isotherm is a 'type I' isotherm as demonstrated by the steep rise in the adsorbed volume of N$_2$, referring the low level of microporosity.[43] The specific surface area, pore volume, and average pore size of SDCC-NiO were found to be 12.6 m^2 g^{-1}, 0.036 cm^2 g^{-1}, and 4.79 nm, respectively.

XRD measurements for SDCC-NiO were recorded from an angle ($2\theta = 10°$ to $90°$). The XRD patterns of SDCC-NiO matched well with reported literature.[44] This proved the successful synthesis of SDCC-NiO. The XRD patterns of the composite are shown in Fig. 1(c). The diffraction peaks were indexed at $2\theta = 37.2°, 43.2°, 43.45°, 62.8°, 75.4°$, and $79.4°$, which correspond to the N(110), C(101), N(200), N(220), N(311), and N(222) reflections of the composite, respectively (JCPDS card no. 47-1049). The XRD pattern for SDCC-NiO was the same as that for NiO due to
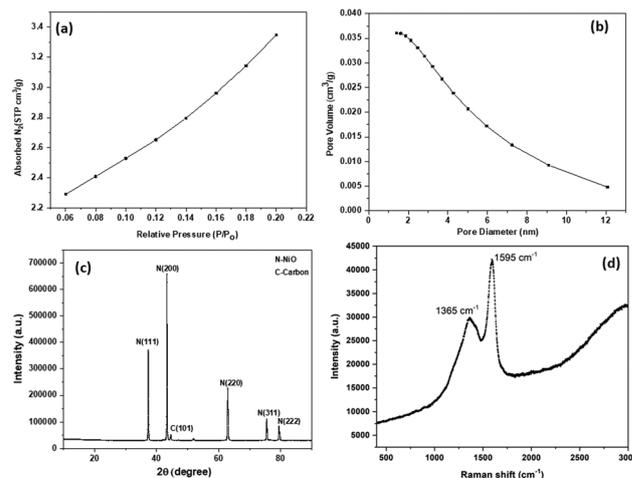

Fig. 1 (a) Nitrogen adsorption/desorption isotherms, (b) nitrogen desorption/desorption pore size distribution, (c) XRD patterns, and (d) Raman spectrum of SDCC-NiO.

the carbons with an amorphous structure derived from sucrose. This result was in agreement with the previously reported result.[44] Also, the structure of NiO in SDCC-NiO can be seen to maintain high crystalline quality.

The Raman spectrum was recorded at a constant room temperature in the wavelength range from 300 to 3200 cm^{-1}. The incorporation of carbon could be confirmed by the Raman spectrum, as shown in Fig. 1(d). The carbon derived from sucrose could be characterized by the G peak at 1595 cm^{-1} and the D peak at 1365 cm^{-1}, which were due to the E_{2g} phonon of the sp^2 hybridization and the disorder originating from the defected sites of the carbon structure, respectively.[45–47] Obviously, SDCC-NiO was Raman active and presented a Raman spectrum similar to that of sucrose-derived carbon, indicating the existence of carbon derived from sucrose in SDCC-NiO. The intensity ratio of the D and G peaks (I_D/I_G) can be employed to evaluate the quality of the graphite crystal structures. Compared to the carbon derived from sucrose in previous study,[45] the lower the I_D/I_G value (0.71) of SDCC-NiO more the graphitization in carbon derived from sucrose after interaction with NiO.[48–51]

SDCC-NiO was covered by carbon derived from sucrose and the size of most of the composites was smaller than those of the parental ones due to the limited crystal growth space between carbon layers and the influence of carbon derived from sucrose

on nucleation rate, indicating the composition of carbon and NiO.

The morphology and structure of SDCC-NiO were investigated *via* scanning electron microscopy (SEM) and transmission electron microscopy (TEM). The SEM images in Fig. 2(a) and (b) depicted the morphology of SDCC-NiO and exhibited SDCC-NiO as the aggregates of particles with a small particle size in the range of less than few microns, while some of the particles seemed bigger having size more than 100 μm. The TEM analysis was performed to further characterize the detailed morphology and microstructure of the composite. As shown in Fig. 2(d), the TEM image indicates a uniform distribution of carbon coating on NiO nanoparticles. The SAED pattern (Fig. 2(f)) indicates polycrystalline nature of overall NiO nanoparticles. The three marked diffraction rings correspond to the {111}, {200}, and {220} planes, respectively.

XPS analysis was done for investigating the chemical component and electronic states of SDCC-NiO, as shown in Fig. 3. In the XPS analysis, the Al Kα line was used as the X-ray source. Only Ni, C, and O elements were found from the XPS survey spectra analyses (Fig. 3(a)). A typical Ni 2p XPS spectrum is shown in Fig. 3(b). It is observed that due to the spin–orbit effect, the peak of Ni 2p is mainly composed of Ni 2p$_{1/2}$ and Ni 2p$_{3/2}$. The peaks located at 855.5 eV with a satellite at 861.0 eV and 872.8 eV with a satellite at 879.4 eV may be attributed to Ni^{2+} 2p$_{3/2}$ and Ni^{2+} 2p$_{1/2}$, respectively, indicating the presence of NiO.[52,53] The results indicated that the chemical structure of NiO formed in the carbonization process was in agreement with the above XRD results.

As shown in Fig. 3(c), three peaks for O 1s are observed at 530.1 eV, 532.0 eV, and 533.6 eV, which are associated with O 1s binding energies of O–Ni, O–H, and O–C, respectively.[54,55]

In the C 1s spectrum of the composite, four characteristic peaks were observed at 284.7 eV, 286.5 eV, 288.5 eV, and 290.5 eV, resulting from the C–C, C–O, C=O, and O–C=O units, respectively, as demonstrated in Fig. 3(d).[56]
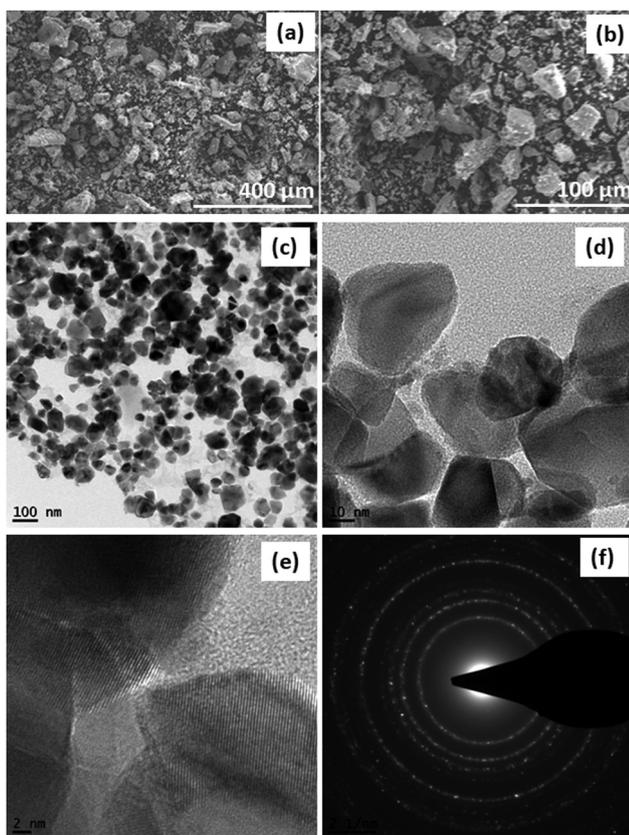

Fig. 2 SEM images of SDCC–NiO (a) at low magnification, (b) at high magnification, (c) TEM image at low magnification, (d and e) TEM image at high magnification, and (f) SAED patterns of SDCC–NiO.
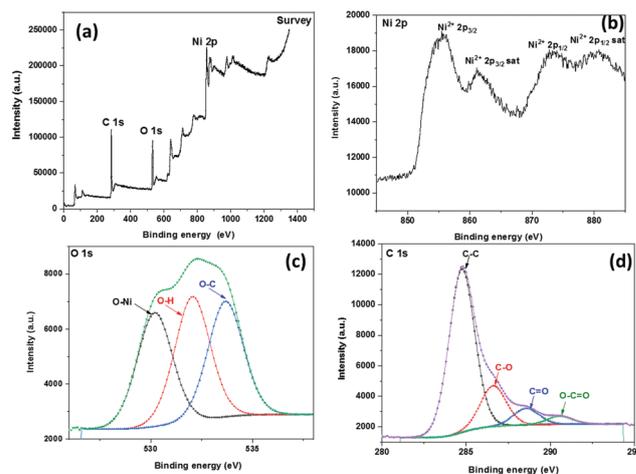

Fig. 3 XPS of SDCC–NiO (a) survey scan, (b) Ni 2p spectrum, (c) O 1s spectrum, and (d) C 1s spectrum.

3.2. Electrochemical analysis of SDCC-NiO

SDCC-NiO was characterized *via* cyclic voltammetry (CV) and electrochemical impedance spectroscopy (EIS). The CV experiments were performed at the scan rates ranging between 5 and 50 mV s^{-1} in the potential window of 0.0 to +0.6 V, as demonstrated in Fig. 4(a). The CV loops were observed in a shape close to a rectangle, which is desirable for a supercapacitor. In the redox process, the following reaction (1) takes place:

$$NiO + OH^- \rightarrow NiOOH + e^- \tag{1}$$

NiO exhibits redox pseudocapacitance, which refers to the adsorption of ions onto the surface of the active electrode material. For NiO, redox pseudocapacitance would be mainly from the ions adsorbing onto the surface instead of inserting into the material similar to that of MnO_2.[57,58] Therefore, the rectangle-shaped CV curves were obtained from the SDCC-NiO composite electrode.

The following eqn (2) was used to calculate the specific gravimetric capacitance (C, F g^{-1}) of the SDCC-NiO electrode from the CV curves.[59]

Energy density (E) and power density (P) are expressed as shown in the following eqn (3) and (4):

$$E \text{ (W h kg}^{-1}) = \tfrac{1}{2} \times C \times (\Delta V)^2 \times 1000/3600 \tag{3}$$

$$P \text{ (W kg}^{-1}) = E/\Delta t \tag{4}$$

C is the specific capacitance calculated from the CV curves.

The specific capacitance as a function of the scan rate for SDCC-NiO is shown in Fig. 4(b), and it is observed that the value of the specific capacitance decreases with the increase in the scan rate. The maximum value of the specific capacitance is observed as 473 F g^{-1} at a scan rate of 5 mV s^{-1}, while the minimum value of specific capacitance is observed as 73 F g^{-1} at a scan rate of 50 mV s^{-1}.

Actually, the rate capability of the electrode is governed by three processes: ion mobility in the electrolyte, the diffusion and surface adsorption of ions on the electrode, and the charge transfer between the electrode and electrolyte ions.[61] At larger scan rates, any of the above processes is relatively slow and the electrode is not utilized completely to store the charge. It limits the rate capability of the system, and hence decreases specific

$$C = \frac{\text{Area under the CV curve (mA V)}}{2 \times \text{scan rate} \left(\dfrac{\text{mV}}{\text{s}}\right) \times \text{potential window (V)} \times \text{mass of working electrode (g)}} \tag{2}$$
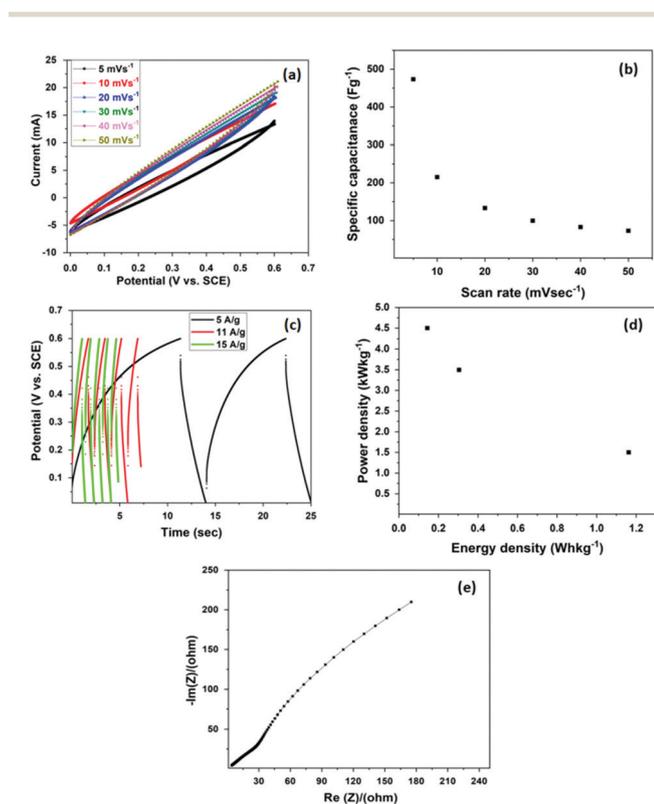
capacitance.[61] The SDCC-NiO electrode retains about 16% of capacitance at a scan rate of 50 mV s^{-1}. The retention of capacitance at such higher scan rates is attributed to the advantages of the SDCC-NiO composite.[62] The nanoparticles of NiO may accommodate more ions from the electrolyte exhibiting higher redox pseudocapacitance during the charging/discharging processes. Moreover, sucrose-derived carbon (SDC) also contributes to the total specific capacitance of SDCC-NiO. In addition, it also exhibits good electronic conductivity and thus works as a supporting channel for electrons between NiO particles.[62–64] Therefore, combining these two materials into a single electrode improved the electrochemical properties for supercapacitor applications. The SDCC-NiO composite exhibited larger capacitance as compared to NiO/carbon fabric electrode[65] and the carbon–metal oxide composite electrode reported previously.[63,66]

To confirm the electrochemical properties of SDCC-NiO, galvanostatic charge–discharge (GCD) measurements were performed. Fig. 4(c) shows the GCD curves measured at various applied currents 5, 11, and 15 A g^{-1}, respectively. Similar to the results of CV curves, the GCD results also verify the capacitive behavior of the samples. The charge and discharge curves were observed to be almost symmetric, exhibiting an ideal capacitive behavior, which is a typical normal characteristic of an ideal capacitor with good electrochemical phenomena.[58,67]

The specific capacitance from the galvanostatic charge–discharge curve was calculated using the following eqn (5) reported in the literature:

$$C = I \times \Delta t / \Delta V \times m \tag{5}$$

Fig. 4 (a) CV curves recorded at the scan rates of 5, 10, 20, 30, 40, and 50 mV s^{-1}, (b) specific capacitance as a function of the scan rate, (c) charging and discharging curves recorded at the current densities of 5, 11, and 15 A g^{-1}, (d) energy density *vs.* power density (Ragone plot), and (e) Nyquist plot of SDCC-NiO.

where I is the applied discharge current, Δt is the discharged time, m is the mass on the electrode and ΔV is the potential window in GCD measurements.

The specific capacitance values of SDCC-NiO were calculated at different current densities. At the current density of 5 A g^{-1}, the specific capacitance was 23.25 F g^{-1}. The capacitance decreased to 8.62 F g^{-1} at a current density of 15 A g^{-1}. As the current density is increased, the specific capacitance generally decreases. It could be because of the slow adsorption of ions on the electrode surface at a higher current density and hence the active ionic species are not fully utilized, leading to the decrease in the capacitance of the electrode.[59,60]

Energy and power densities were determined from GCD measurements at different currents and are represented in the Ragone plot (Fig. 4(d)). The Ragone plot shows that the power density increases and energy density decreases with the current density. The power density and energy density of the SDCC-NiO electrode were found to be 0.14 W h kg^{-1} and 4.5 kW kg^{-1} at the current density of 15 A g^{-1}, respectively.

Further, electrochemical impedance spectroscopy (EIS) was used to investigate the electrochemical performance of the SDCC-NiO electrode. Fig. 4(e) depicts the Nyquist plots of the electrode, as obtained from EIS analyses. The EIS experiment was performed in the frequency range from 0.1 Hz to 100 kHz with an ac amplitude of 5 mV. The real component in the Nyquist plots is associated with the resistive nature of the sample, while the imaginary part shows the capacitive nature of the electrode. At very high frequencies, the electrode behaves like a resistor, while at low frequencies it exhibits a pure capacitive nature. As the frequency decreases, the resistance (R) decreases and the capacitance (C) becomes more effective.[61]

Warburg impedance is also observed at the low-frequency region. The linear region is not exactly parallel to the imaginary axis, indicating that the electrode process is not perfectly capacitive but it is diffusion-controlled.[60,68] The Warburg impedance is associated with the frequency-dependent ionic diffusion of ions from electrolyte onto the electrode. The first intersection at the real axis represents the effective series resistance (ESR).[58] Series resistance (R_s) includes solution resistance, the intrinsic resistance of the current collector and active electrode material, and contact resistance between the electrode and current collector. It must be minimized for high-performance supercapacitors. In our case, the series resistance of the SDCC-NiO electrode was determined to be 4.2 Ohms. On the basis of this study, we may suggest that there is a possibility of extending the sucrose-derived carbon-based coating to other oxides such as CuO, VO$_2$, and MgO, which could broaden the area of smart green carbon coating technological applications.[69–71]

4. Conclusions

Sucrose-derived carbon-coated nickel oxide (SDCC-NiO) was successfully synthesized via a colloidal method and investigated for high-performance supercapacitor applications. SDCC-NiO was prepared with the soluble source of carbon (sucrose) and nickel oxide nanoparticles. The soluble source of carbon was converted into carbon during annealing in an inert atmosphere and coated on nickel oxide particles. SDCC-NiO showed a specific capacitance of 473 F g^{-1} in a three-electrode system at a scan rate of 5 mV s^{-1} in a 1 M KOH electrolyte. The electrochemical results demonstrate that the SDCC-NiO electrode has high capacitance with high power and moderate energy density. The as-synthesized SDCC-NiO may be a promising candidate for high-performance supercapacitors.

Conflicts of interest

There are no conflicts of interest to declare.

Acknowledgements

References

1 P. G. Bruce, S. A. Freunberger, L. J. Hardwick and J. M. Tarascon, Li–O$_2$ and Li–S Batteries with High Energy Storage, *Nat. Mater.*, 2012, **11**, 19–29.

2 Y. Zhang, H. Feng, X. Wu, L. Wang, A. Zhang, T. Xia, H. Dong, X. Li and L. Zhang, Progress of electrochemical capacitor electrode materials: a review, *Int. J. Hydrogen Energy*, 2009, **34**, 4489–4499.

3 L. L. Zhang and X. S. Zhao, Carbon-based materials as supercapacitor electrodes, *Chem. Soc. Rev.*, 2009, **38**, 2520–2531.

4 M. Khenfouch, R. M. Ndimba, A. Diallo, S. Khamlich and M. Hamzah, Artemisia herba-alba Asso eco-friendly reduced few-layered graphene oxide nanosheets: structural investigations and physicalproperties, *G. Chem. Lett. Rev.*, 2016, **9**, 122–131.

5 S. Khamlich, T. Khamliche, M. S. Dhlamini, M. Khenfouch and B. M. Mothudi, Rapid microwave-assisted growth of silver nanoparticles on 3D graphene networks for supercapacitor application, *J. Colloid Interface Sci.*, 2017, **493**, 130–137.

6 E. Ismail, S. Khamlich, M. Dhlamini and M. Maaza, Green biosynthesis of ruthenium oxide nanoparticles on nickel foam as electrode material for supercapacitor applications, *RSC Adv.*, 2016, **6**, 86843–86850.

7 S. Khamlich, T. Mokrani, M. S. Dhlamini, B. M. Mothudi and M. Maaza, Microwave-assisted synthesis of simonkolleite nanoplatelets on nickel foam–graphene with enhanced surface area for high-performance supercapacitors, *J. Colloid Interface Sci.*, 2016, **461**, 154–161.

8 Y. R. Ahn, M. Y. Song, S. M. Jo, C. R. Park and D. Y. Kim, Electrochemical capacitors based on electrodeposited ruthenium oxide on nanofibre substrates, *Nanotechnology*, 2006, **17**, 2865–2869.

9 J. Yan, T. Wei, J. Cheng, Z. Fan and M. Zhang, Preparation and electrochemical properties of lamellar MnO$_2$for supercapacitors, *Mater. Res. Bull.*, 2010, **45**, 210–215.

10 Y. Zhao and C. A. Wang, Nano-network MnO$_2$/polyaniline composites with enhanced electrochemical properties for supercapacitors, *Mater. Des.*, 2016, **97**, 512–518.

11 S. G. Kandalkar, J. L. Gunjakar and C. D. Lokhande, Preparation of cobalt oxide thin films and its use in supercapacitor application, *Appl. Surf. Sci.*, 2008, **254**, 5540–5544.

12 N. Matinise, N. Mayedwa, X. G. Fuku, N. Mongwaketsi and M. Maaza, Green synthesis of cobalt(II, III) oxide nanoparticles using Moringa Oleifera natural extract as high electrochemical electrode for supercapacitors, *AIP Proc.*, 1962, **2018**, 040005.

13 S. Khamlich, Z. Abdullaeva, J. V. Kennedy and M. Maaza, High-performance symmetric supercapacitor based on zinc hydroxychloride nanosheets and 3D graphene-nickel foam composite, *Appl. Surf. Sci.*, 2017, **405**, 329–336.

14 G. T. Anand, D. Renuka, R. Ramesh, L. Anandaraj and S. J. Sundaram, Green synthesis of ZnO nanoparticle using Prunus dulcis (Almond Gum) for antimicrobial and supercapacitor applications, *Surf. Interfaces*, 2019, **17**, 100376.

15 S. Khamlich, Z. Abdullaeva, J. V. Kennedy and M. Maaza, High performance symmetric supercapacitor based on zinc hydroxychloride nanosheets and 3D graphene-nickel foam composite, *Appl. Surf. Sci.*, 2017, **405**, 329–336.

16 R. Kumar, R. K. Nekouei and V. Sahajwalla, *In situ* carbon-coated tin oxide (ISCC-SnO$_2$) for micro-supercapacitor applications, *Carbon Lett.*, DOI: 10.1007/s42823-020-00142-0.

17 R. Kumar, B. K. Singh, A. Soam, S. Parida, V. Sahajwalla and P. Bhargava, In situ carbon supported titanium dioxide (ICS-TiO$_2$) as electrode material for high performance supercapacitors, *Nanoscale Adv.*, 2020, **2**, 2376–2386.

18 R. Kumar, M. Singh and A. Soam, Study on electrochemical properties of silicon micro particles as electrode for supercapacitor application, *Surf. Interfaces*, 2020, **19**, 100524.

19 A. Soam, R. Kumar, D. Thatoi and M. Singh, Electrochemical Performance and Working Voltage Optimization of Nickel Ferrite/Graphene Composite based Supercapacitor, *J. Inorg. Organomet. Polym. Mater.*, DOI: 10.1007/s10904-020-01540-7.

20 G. Wang, L. Zhang and J. Zhang, A review of electrode materials for electro-chemical supercapacitors, *Chem. Soc. Rev.*, 2012, **41**, 797–828.

21 T. Girija and M. Sangaranarayanan, Polyaniline-based nickel electrodes for electrochemical supercapacitors—Influence of Triton X-100, *J. Power Sources*, 2006, **159**, 1519–1526.

22 K. Lota, V. Khomenko and E. Frackowiak, Capacitance properties of poly(3,4-ethylenedioxythiophene)/carbon nanotubes composites, *J. Phys. Chem. Solids*, 2004, **65**, 295–301.

23 J. Y. Kim, K. H. Kim and K. B. Kim, Fabrication and electrochemical properties of carbon nanotube/polypyrrole composite film electrodes with controlled pore size, *J. Power Sources*, 2008, **176**, 396–402.

24 L. Zhang, D. Shi, T. Liu, M. Jaroniec and J. Yu, Nickel based materials for supercapacitors, *Mater. Today*, 2019, **25**, 35–65.

25 M. Wu, Y. Lin, C. Lin and J. Lee, Formation of nano-scaled crevices and spacers in NiO-attached graphene oxide nanosheets for supercapacitors, *J. Mater. Chem.*, 2012, **22**, 2442–2448.

26 B. Dong, H. Zhou, J. Liang, L. Zhang, G. Gao and S. Ding, One-step synthesis of free-standing α-Ni(OH)$_2$ nanosheets on reduced graphene oxide for high-performance supercapacitors, *Nanotechnology*, 2014, **25**, 435403.

27 M. Jing, C. Wang, H. Hou, Z. Wu, Y. Zhu, Y. Yang, X. Jia, Y. Zhang and X. Ji, Ultrafine nickel oxide quantum dots embedded with few-layer exfoliative graphene for an asymmetric supercapacitor: enhanced capacitances by alternating voltage, *J. Power Sources*, 2015, **298**, 241–248.

28 Y. H. Lin, T. Y. Wei, H. C. Chien and S. Y. Lu, Manganese oxide/carbon aerogel composite: an outstanding supercapacitor electrode material, *Adv. Energy Mater.*, 2011, **1**, 901–907.

29 G. Yu, L. Hu, M. Vosgueritchian, H. Wang, X. Xie, J. R. McDonough, X. Cui, Y. Cui and Z. Bao, Solution-Processed Graphene/MnO$_2$ Nanostructured Textiles for High-Performance Electrochemical Capacitors, *Nano Lett.*, 2011, **11**, 2905–2911.

30 Q. T. Qu, S. B. Yang and X. L. Feng, 2D Sandwich-like Sheets of Iron Oxide Grown on Graphene as High Energy Anode Material for Supercapacitors, *Adv. Mater.*, 2011, **23**, 5574–5580.

31 Z. Zhang, Q. Gao, H. Gao, Z. Shi, J. Wu., M. Zhi and Z. Hong, Nickel oxide aerogel for high performance supercapacitor electrodes, *RSC Adv.*, 2016, **6**, 112620–112624.

32 B. Yuan, C. Xu, D. Deng, Y. Xing, L. Liu, H. Pang and D. Zhang, Graphene oxide/nickel oxide modified glassy carbon electrode for supercapacitor and nonenzymatic glucose sensor, *Electrochim. Acta*, 2013, **88**, 708–712.

33 Q. Liu, C. Lu and Y. Li, Controllable synthesis of ultrathin nickel oxide sheets on carbon cloth for high performance supercapactiors, *RSC Adv.*, 2017, **7**, 23143–23148.

34 X. Zhu, H. Dai, J. Hu, L. Ding and L. Jiang, Reduced graphene oxide-nickel oxide composite as high performance electrode materials for supercapacitors, *J. Power Sources*, 2012, **203**, 243–249.

35 F. I. Dar, K. R. Moonooswamy and M. Es-Souni, Morphology and property control of NiO nanostructures for supercapacitor applications, *Nanoscale Res. Lett.*, 2013, **8**, 363–369.

36 C. Wang, J. Xu, M. F. Yuen, J. Zhang, Y. Li, X. Chen and W. Zhang, Hierarchical composite electrodes of nickel Oxide Nanoflake 3D graphene for high-performance pseudocapacitors, *Adv. Funct. Mater.*, 2014, **24**, 6372–6380.

37 X. Sun, G. Wang, J. Y. Hwang and J. Lian, Porous nickel oxide nano-sheets for high performance pseudocapacitance materials, *J. Mater. Chem.*, 2011, **21**, 16581–16588.

38 D. C. Iwueke, C. I. Amaechi, A. C. Nwanya, A. B. C. Ekwealor and P. U. Asogwa, A novel chemical preparation of Ni(OH)$_2$/CuO nanocomposite thin films for supercapacitive applications, *J. Mater. Sci.: Mater. Electron.*, 2015, **26**, 2236–2242.

39 R. Kumar and P. Bhargava, Synthesis and Characterization of low specific resistance alumina-clay-carbon composites by colloidal processing using sucrose as a soluble carbon source for electrical applications, *RSC Adv.*, 2016, **6**, 8705–8713.

40 R. Kumar and P. Bhargava, Fabrication of low specific resistance ceramic carbon composites by colloidal processing using

glucose as soluble carbon source, *Bull. Mater. Sci.*, 2017, **40**, 1197–1202.

41 R. Kumar, B. K. Singh, A. Soam, S. Parida and P. Bhargava, *In situ* carbon coated manganese oxide nanorods (ISCC-MnO$_2$NRs) as an electrode material for supercapacitors, *Diamond Relat. Mater.*, 2019, **94**, 110–117.

42 R. Kumar, Parag Bhargava,Fabrication of low specific resistance ceramic carbon composites by slip casting, *Asian Ceram. Soc.*, 2015, **3**, 262–265.

43 P. D. Dietzel, B. Panella, M. Hirscher, R. Blom and H. Fjellvåg, Hydrogen adsorption in a nickel based coordination polymer with open metal sites in the cylindrical cavities of the desolvated framework, *Chem. Commun.*, 2006, 959–961.

44 J. W. Lee, T. Ahn, J. H. Kim, J. M. Ko and J. D. Kim, Nanosheets based mesoporous NiO microspherical structures via facile and template-free method for high performance supercapacitors, *Electrochim. Acta*, 2011, **56**, 4849–4857.

45 R. Kumar, A. Soam, R. O. Dusane and P. Bhargava, Sucrose derived carbon coated silicon nanowires for supercapacitor application, *J. Mater. Sci.: Mater. Electron.*, 2018, **29**, 1947–1954.

46 R. Kumar, A. Raj, S. Mitra and P. Bhargava, Carbon derived from sucrose as anode material for lithium-ion batteries, *J. Electron. Mater.*, 2019, **48**, 7389–7395.

47 R. Kumar, S. S. Nemala, S. Mallick and P. Bhargava, Synthesis and characterization of carbon based counter electrode for dye sensitized solar cells (DSSCs) using sugar free as a carbon material, *Sol. Energy*, 2017, **144**, 215–220.

48 R. Kumar and P. Bhargava, Fabrication of a counter electrode using glucose as carbon material for dye sensitized solar cells, *Mater. Sci. Semicond. Process.*, 2015, **40**, 331–336.

49 R. Kumar and P. Bhargava, Synthesis and characterization of carbon based counter electrode for dye sensitized solar cells (DSSCs) using organic precursor 2-2′ Bipyridine (Bpy) as a carbon material, *J. Alloys Compd.*, 2018, **748**, 905–910.

50 R. Kumar, V. Sahajwalla and P. Bhargava, Fabrication of a counter electrode for dye-sensitized solar cells (DSSCs) using carbon material produced by organic ligand 2-Methyl-8-hydroxyquinolinol (Mq), *J. Nanoscale Adv.*, 2019, **1**, 3292–3299.

51 Y. Wu, H. Luo and H. Wang, Synthesis of iron(III)-based metal-organic framework/graphene oxide composites with increased photocatalytic performance for dye degradation, *RSC Adv.*, 2014, **4**, 40435–40438.

52 M. Madkour, Y. K. Abdel-Monem and F. Al Sagheer, Controlled synthesis of NiO and Co$_3$O$_4$ nanoparticles from different coordinated precursors: impact of precursor's geometry on the nanoparticles characteristics, *Ind. Eng. Chem. Res.*, 2016, **55**, 12733–12741.

53 C. Wang, B. Tian, W. Mei and J. Wang, Revelation of its excellent intrinsic activity of MoS$_2$/NiS/MoO$_3$ nanowire for hydrogen evolution reaction in alkaline medium, *ACS Appl. Mater. Interfaces*, 2017, **9**, 7084–7090.

54 L. C. Lopez, D. W. Dwight and M. B. Polk, The $\pi \rightarrow \pi^*$ shake-up phenomena in polyesters containing backbone aromatic groups, *Surf. Interface Anal.*, 1986, **9**, 405–409.

55 J. Haber, J. Stoch, L. Ungier, J. Haber, J. Stoch and L. Ungier, X-ray photoelectron spectra of oxygen in oxides of Co, Ni, Fe and Zn, *J. Electron Spectrosc. Relat. Phenom.*, 1976, **9**, 459–467.

56 H. Q. Wang, J. Chen, S.-J. Hu, X.-H. Zhang, X.-P. Fan, J. Du, Y.-G. Huang and Q.-Y. Li, Direct growth of flower-like 3D MnO$_2$ ultrathin nanosheets on carbon paper as efficient cathode catalyst for rechargeable Li–O$_2$ batteries, *RSC Adv.*, 2015, **5**, 72495–72499.

57 J. Deng, M. R. Nellist, M. B. Stevens, C. Dette, Y. Wang and S. W. Boettcher, Morphology Dynamics of Single-Layered Ni(OH)$_2$/NiOOH Nanosheets and Subsequent Fe Incorporation Studied by *in situ* Electrochemical Atomic Force Microscopy, *Nano Lett.*, 2017, **17**(11), 6922–6926.

58 A. Soam, K. Parida, R. Kumar, P. Kavle and R. O. Dusane, Silicon-MnO$_2$ core-shell nanowires as electrodes for micro-supercapacitor application, *Ceram. Int.*, 2019, **45**, 18914–18923.

59 U. Kumar, V. Gaikward, M. Mayyas, V. Sahajwalla and R. Joshi, Extraordinary supercapacitance in activated carbon produced *via* a sustainable approach, *J. Power Sources*, 2018, **394**, 140–147.

60 X. Dai, M. Zhang, J. Li and D. Yang, Effects of electrodeposition time on a manganese dioxide supercapacitor, *RSC Adv.*, 2020, **10**, 15860–15869.

61 N. Kumar, A. Kumar, G. M. Huang, W. W. Wu and T. Y. Tsen, Facile synthesis of mesoporous NiFe$_2$O$_4$/CNTs nanocomposite cathode material for high performance asymmetric pseudocapacitors, *Appl. Surf. Sci.*, 2018, **433**, 1100–1112.

62 M. Zhi, C. Xiang, J. Li, M. Li and N. Wu, Nanostructured carbon–metal oxide composite electrodes for supercapacitors: a review, *Nanoscale*, 2013, **5**, 72–88.

63 A. Soam, R. Kumar, C. Mahender, M. Singh, D. Thatoi and R. O. Dusane, Development of paper-based flexible supercapacitor: Bismuth ferrite/graphene nanocomposite as an active electrode material, *J. Alloys Compd.*, 2020, **813**, 152145.

64 B. T. Sone, X. G. Fuku and M. Maaza, Physical & Electrochemical Properties of Green Synthesized Bunsenite NiO Nanoparticles via Callistemon Viminalis' Extracts, *Int. J. Electrochem. Sci.*, 2016, **11**, 8204–8220.

65 Y. L. Tai and H. S. Tang, Modification of porous carbon with nickel oxide impregnation to enhance the electrochemical capacitance and conductivity, *Carbon*, 2004, **42**, 2335–2338.

66 J. Yan, Z. Fan, T. Wei, W. Qian, M. Zhang and F. Wei, Fast and reversible surface redox reaction of graphene–MnO$_2$ composites as supercapacitor electrodes, *Carbon*, 2010, **48**, 3825–3833.

67 A. Soam, R. Kumar, P. K. Sahoo, C. Mahender, B. Kumar, N. Arya, M. Singh, S. Parida and R. O. Dusane, Synthesis of Nickel Ferrite Nanoparticles Supported on Graphene Nanosheets as Composite Electrodes for High Performance Supercapacitor, *ChemistrySelect*, 2019, **4**, 9952–9958.

68 A. Chidembo, S. H. Aboutalebi, K. Konstantinov, M. Salari, B. Winton, S. A. Yamini, I. P. Nevirkovets and H. K. Liu,

Globular reduced graphene oxide-metal oxide structures for energy storage applications, *Energy Environ. Sci.*, 2012, **5**, 5236–5240.

69 M. Maaza, O. Nemraoui, C. Sella and A. C. Beye, Surface Plasmon Resonance Tunability in Au–VO₂ Thermochromic Nano-composites, *Gold Bull.*, 2005, **38**, 100–106.

70 K. Kaviyarasu, C. M. Magdalane, K. Anand, E. Manikandan and M. Maaza, Synthesis and characterization studies of MgO:CuO nanocrystals by wet-chemical method, *Spectrochim. Acta, Part A*, 2015, **142**, 405–409.

71 A. Simo, B. Mwakikunga, B. T. Sone, B. Julies, R. Madjoe and M. Maaza, *Int. J. Hydrogen Energy*, 2014, **39**, 8147–8157.